Nuclear Instruments and Methods 205 (1983) 125–132
North-Holland Publishing Company

THE ARGUS ELECTRON–PHOTON CALORIMETER
I. Detection of low-energy electromagnetic showers

A. DRESCHER, B. GRÄWE, W. HOFMANN, A. MARKEES, U. MATTHIESEN, D. POLLMANN, J. SPENGLER and D. WEGENER

Institut für Physik der Universität Dortmund, Otto-Hahn Strasse, 4600 Dortmund, Germany

Received 28 May 1982

The performance of the ARGUS shower counters in detecting electromagnetic showers in the energy range 10–45 MeV is reported. When these results are considered with earlier measurements at GeV energies, it is seen that the device behaves almost like an ideal calorimeter over three decades in energy, with good linearity and a $1/\sqrt{E}$ dependence of the energy resolution. The detection threshold is at least as low as 10 MeV.

Characteristics of low-energy electromagnetic showers, such as longitudinal shower profile and fraction of energy visible in the scintillator were measured, and are compared with results obtain from the EGS Monte Carlo code.

1. Introduction

In the ARGUS detector, which is built for the electron–positron storage ring DORIS II at DESY, a system of lead scintillator sampling shower counters with nearly 4π acceptance is used to detect electrons and photons. The physical prospects of the experiment require an electromagnetic calorimeter, which has very good energy resolution, spatial homogeneity, and high detection efficiency for low-energy photons and electrons combined with the ability to reconstruct the impact point of a particle with reasonable accuracy.

These goals can only be achieved by placing the calorimeter inside the solenoid coil of the ARGUS detector. The calorimeter consists of a cylindrical "barrel" counter and two "endcap" parts and is segmented into 1760 modules, each read out via its own wave shifter plate [1]. The design provides both fine sampling and extensive segmentation with minimal dead space.

In two earlier papers [2,3] we have reported tests of prototype shower counters. In the present work, we will present results on the detection of very low energy electrons in the 10–40 MeV range using the final calorimeter modules. The paper is subdivided as follows: in section 2, the design of the counter modules is discussed. In section 3, some "fundamental" question like linearity at very low electron energies, and $1/\sqrt{E}$ dependence of the energy resolution are addressed. Section 4 concentrates on more "practical" aspects: homogeneity, energy- and spatial resolution averaged over the entire area of the detector, and over various angles of incidence. Finally, a brief summary is given in section 5.

2. The lead/scintillator counter modules

The test setup consisted of several identical calorimeter modules arranged in a matrix. The construction of one module is shown in fig. 1. Each module contains two separate counters, that is two separate stacks of alternate layers of 5 mm plastic scintillator [4] and 1 mm lead plates. The front area of a module (both counters) covers 22.5×11 cm^2, its depth is approx. 40 cm, or 12.5 radiation lengths.

The two stacks are read out separately via two wavelength-shifter bars [5] of 3 mm thickness placed between the two stacks, in the middle of each module. The re-emitted scintillator light is collected by adiabatic light guides and is fed into a 1″ photomultiplier [6]. The two wavelength shifters are optically separated by aluminized mylar foil to eliminate crosstalk. A 0.3 mm nylon thread serves to maintain the air gap between wavelength shifter and absorber stack, which is required to ensure the total internal reflection of light trapped in the shifter bar. The whole module is wrapped in aluminum foil, and covered by four layers of thermal shrink tubing [7]. Although each of these layers has only 30 μm thickness, this procedure yields a good mechanical stability. The tubing is black, and so also guarantees the light tightness of the assembly, its transmission being less than 10^{-7}. Front and rear ends of each module are covered by 3 mm thick black plexiglass plates. All edges are further protected by adhesive tape. A more detailed description of construction and machining of the calorimeter modules will be given elsewhere [8].

0167-5087/83/0000–0000/$03.00

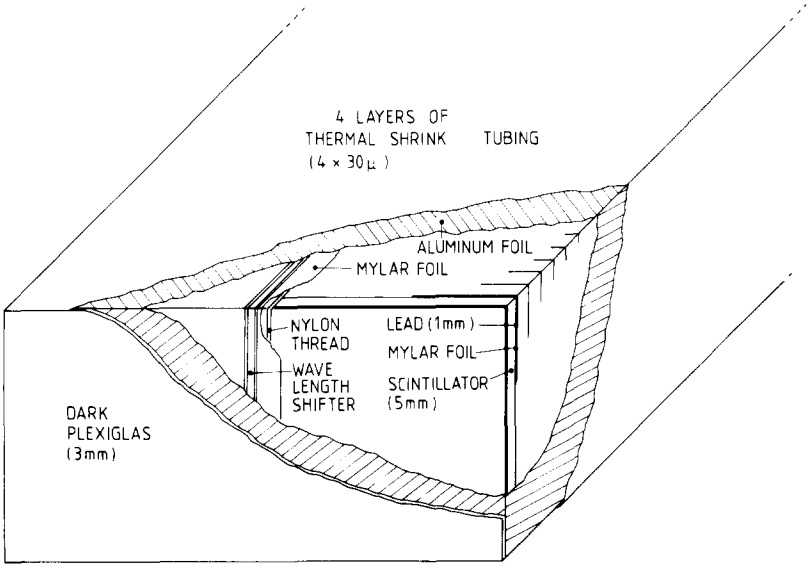

Fig. 1. Construction of a shower counter module: One module contains two stacks of lead- and scintillator plates, each of which is read out by its own wave shifter plate. All edges are taped for extra protection.

In the ARGUS barrel shower counter, two types of modules are used: modules like the one shown in fig. 1 alternate with conical-shaped modules. In the present test, only modules of the first type were used. The special properties of the conical modules will be described in a forthcoming paper on the light collection system of the shower counters [9].

For the tests described in this paper, the calorimeter modules were exposed to an external electron beam of the Dortmund Betatron. The data presented in section 3 were taken under optimum beam conditions at a very low rate. For the less critical data discussed in section 4, the trigger conditions were loosened in order to increase the rate, resulting in a few percent false triggers at energies below 30 MeV.

For comparison, some figures include data taken at higher energies at the Bonn Synchrotron and at DESY. Fig. 2 illustrates how the energy deposition in showers changes when going from Betatron to DESY energies. The profile of an electromagnetic shower at Betatron energies (< 40 MeV) is compared to a Monte Carlo simulation produced by the EGS code [10]. To obtain these data, the corresponding scintillator plate in a module was replaced by a probe counter. For comparison, the profile of a 1 GeV shower is also shown. The 39 MeV shower is almost entirely contained in the first third of the calorimeter module.

A first impression of the performance of the calorimeter modules is given by fig. 3, where the distribution of pulse height for 39 MeV electrons is shown. The width of the LED reference line proves that the energy resolution is not limited by photoelectron statistics.

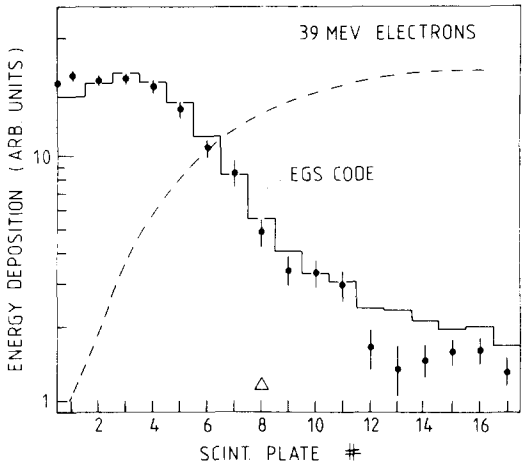

Fig. 2. Longitudinal development of 39 MeV electron showers in the lead/scintillator calorimeter, compared to a Monte-Carlo simulation using the EGS code: The arrow indicates the center of gravity $\bar{z}$ of an average shower, taken from the EGS simulation, $\bar{z}$ is defined as $(\int \mathrm{d}E/\mathrm{d}z\ z\ \mathrm{d}z)/(\int \mathrm{d}E/\mathrm{d}z\ \mathrm{d}z)$, with the z-axis pointing along the shower axis. The discrepancy at large depth is probably due to the fact, that the probe counter (8×8 cm^2) did not cover the entire cross section of the absorber stack, for which the EGS simulation was performed; consequently, some particles in the tail of the lateral distribution will have missed the probe counter. Dotted line: profile of a 1 GeV electron shower [10]; the normalization is arbitrary.

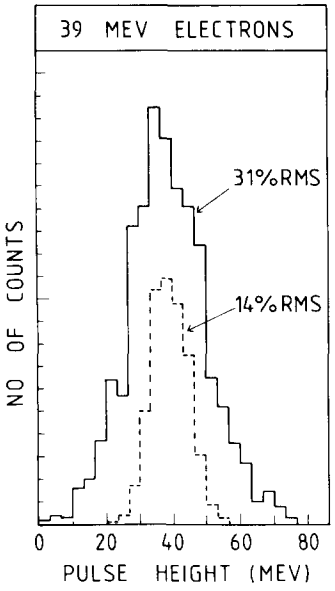

Fig. 3. Distribution of pulse height for 39 MeV electrons incident at the center of an absorber stack: The dotted distribution shows the broadening due to photostatistics of a reference line generated by a pulsed LED at the rear end of the wavelength shifter.

3. Linearity, visible energy, and energy resolution

From considerations of the process of formation of electromagnetic showers, we expect that the response of a calorimeter is a linear function of the energy of incident electrons or photons, and that the intrinsic energy resolution due to sampling fluctuations behaves as $\sigma/E = \text{const.}/\sqrt{E}$ [11]. Even if the resolution is limited by photoelectron statistics, this effect has the same energy dependence, and so the $1/\sqrt{E}$ dependence should be a universal feature of a sampling calorimeter, provided that leakage effects are negligible.

For extermely low energies, however, this behavior does not necessarily continue, since the mechanisms of energy dissipation change. Below the critical energy of the absorber (7 MeV for lead, 80 MeV for scintillator, 12 MeV in average), $\mathrm{d}E/\mathrm{d}x$ dominates the energy loss of the primary electron, and cascade processes are rare. Indeed, deviations from linearity and $1/\sqrt{E}$ dependence have been observed at energies of a few hundred MeV [12].

The experimental investigation of departures from linearity and $1/\sqrt{E}$ dependence requires a precise knowledge of nonlinearities introduced by other components of the test setup, such as

- beam calibration;
- energy loss in trigger counter etc.;
- leakage losses in the calorimeter;
- the longitudinal profile of showers changes with $\ln(E)$; if there exist nonuniformities in the light collection system, the mean efficiency of scintillator light collection may vary;
- nonlinearities in the photomultiplier;
- nonlinearities in the ADCs.

In our case, the accuracy of the calibration of beam energy was measured to be better than 1%. All energy values given are corrected for losses in the trigger counters, the uncertainity of this correction (± 0.35 MeV) is included in the error bars.

Since all data presented in this chapter refer to the energy deposition in a single absorber stack, both longitudinal and lateral leakage cannot be neglected. Therefore, data shown in figs. 5 and 6 are compared to Monte Carlo simulations of electron showers using the EGS code, for exactly the same geometry as in the experiment.

We have carefully checked that the low-energy cut-offs required in the Monte Carlo program do not introduce any bias; for cut-offs below 0.5 MeV and 1.5 MeV for photons and electrons, respectively, stable and consistent results were obtained. The EGS results further show that the amount of leakage – about 1–2% in the longitudinal direction and 12–13% radially – is practically energy independent for electron energies below 100 MeV.

Changes in the efficiency of light collection were corrected for [9]. For the given operating conditions of the multiplier, nonlinearities should be far below 1% [6]. In addition, identical results were obtained for several PMs operated at different gains.

The ADCs [13], however, turned out to be a serious source of nonlinearity, especially when a large dynamic range – from 10 MeV electron showers up to the 150–200 MeV deposited by cosmic muons – was required. The characteristic of the ADCs was measured using a mercury wetted relais, which discharges a capacitor via a passive pulse-shaping network, yielding output impedance and pulse close to the actual PM pulses. The voltage across the capacitor was monitored via a precision DVM. The calibration was done using the final cabling gate width. A good fit of the ADC output (channel no. m) vs. input charge q was obtained by the expression

$$m = Aq + B + Ce^{-Dq} + Ee^{-Fq}. \quad (1)$$

The nonlinearity of the ADC is most easily demonstrated using the slope $\mathrm{d}m/\mathrm{d}q$ of the characteristic. Define $\mathrm{d}m/\mathrm{d}q = 1$ for input charges close to the maximum (256 pC). The first exponential then becomes important for $q < 50$ pC ($\mathrm{d}m/\mathrm{d}q = 0.98$), and reduces $\mathrm{d}m/\mathrm{d}q$ to 0.75 (typically), for $q = 2$ pC. The second exponential sets in at $q < 2$ pC, yielding $\mathrm{d}m/\mathrm{d}q = 0.50$ for $q = 0$. All data were corrected using the characteris-

tic measured for the corresponding ADC channel.

Fig. 4 shows the mean pulse height and the rms energy resolution vs. the kinetic energy of the electrons. Note that "energy resolution" here always refers to the relative width of the distribution, and is quoted in %. The term "normalized resolution" refers to $\sigma\sqrt{E}$. No significant deviations from linearity and $1/\sqrt{E}$ behaviour, respectively, are observed.

In order to check the linearity over a larger range in energy, an independent calibration standard was needed, since the measurements were carried out at different accelerators using different modules. Cosmic muons were used to establish an absolute energy calibration. Given the energy deposition in the scintillator slabs by cosmic muons, one is further able to derive the fraction of visible energy in the scintillator for electromagnetic showers – which is an interesting test quantity for shower models.

In the most naive approach, the fraction of energy deposited in the scintillator, $E_{\text{scint}}/E_{\text{kinetic}}$, is given by

$$\frac{E_{\text{scint}}}{E_{\text{kinetic}}} = \frac{(\mathrm{d}E/\mathrm{d}x)_{\text{scint}} D_{\text{scint}}}{(\mathrm{d}E/\mathrm{d}x)_{\text{lead}} D_{\text{lead}} + (\mathrm{d}E/\mathrm{d}x)_{\text{scint}} D_{\text{scint}}} \quad (2)$$

where D_{scint} and D_{lead} denote the thickness of scintillator and lead plates, respectively.

In real detectors, the fraction of visible energy is reduced by two effects: first, a certain amount of energy leakes out of the detector. Secondly, analytic shower theories [14] state that in the presence of a cut-off energy E_{cut}, below which a track cannot be detected, the visible track length is reduced by a factor $F(E_{\text{cut}}/\epsilon)$, which depends on the critical energy ϵ of the absorber. Hence $E_{\text{scint}}/E_{\text{kin}}$ is reduced by the same factor. In a sampling calorimeter, the energy deposition in a lead-scintillator slab plays the role of a cut-off, since energy measurements are "quantized" in these units; consider e.g. the last piece of the trajectory of an electron, starting at the point where the electron energy decreases below half the energy deposited in one lead–scintillator cell: the chance that this track piece is "lost" before producing a useful "hit" in the scintillator slab is about 50%. In order to show the magnitude of both corrections, fig. 5 presents predictions from approximation-b shower theory [11], and from the EGS Monte Carlo code, for both $E_{\text{scint}}/E_{\text{kin}}$ and $E_{\text{scint}}/E_{\text{deposited}}$. The latter quantity is insensitive to leakage losses, and reflects the influence of the cut-off alone. Based on eq. (2), values of 0.41 and 0.475, respectively, are expected. Fig. 5 includes data pints for $E_{\text{scint}}/E_{\text{kin}}$, obtained at Dortmund Betatron and at DESY energies. The energy deposition by cosmic rays, which is required for normalisation, was calculated by a Monte Carlo simulation

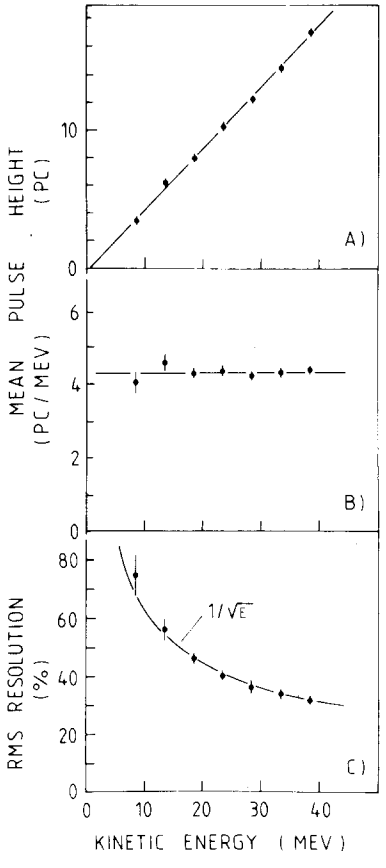

Fig. 4. Mean pulse height (A) absolute, (B) per MeV kinetic energy as a function of the electron energy. The beam hits the absorber stack at its center, and is parallel to the calorimeter axis, (C) Rms energy resolution vs. energy.

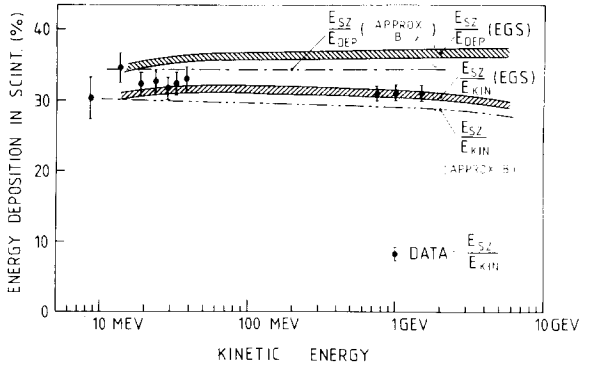

Fig. 5. Fraction of energy deposited in the scintillator, normalized to the kinetic energy of the primary electron, as a function of the electron energy: The error bars shown are dominated by systematic scale errors, which may be different for the low- and high energy groups of data points. Dashed area: EGS predictions for $E_{\text{scint}}/E_{\text{kin}}$ and for $E_{\text{scint}}/E_{\text{dep}}$. Dashed–dotted lines: predictions for $E_{\text{scint}}/E_{\text{kin}}$ and $E_{\text{scint}}E_{\text{dep}}$ using analytical shower theories (approximation b). Typical accuracy: ± 10%.

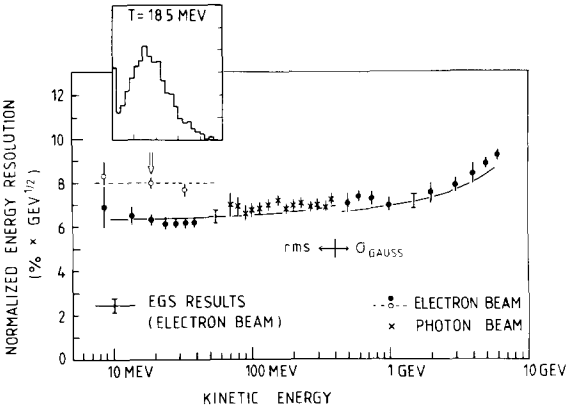

Fig. 6. Normalized energy resolution $\sigma\sqrt{E}$ as a function of energy: Closed points and stars: optimal resolution for central impact parallel to the counter axis. Open points: values averaged over entire surface of the counter array, and over all angles of incidence up to 45°. Low energy points (< 400 MeV) represent true rms values, whereas data points at higher energies refer to a Gaussian fit of the distribution within 1σ around the maximum. The latter method reduces the influence of tails due to leakage. Full line: EGS predictions including leakage and photoelectron statistics. The estimated error of the simulation is indicated. Small insert: distribution of pulse height for 18.5 MeV electrons, averaged over impact points and -angles.

including the cosmic muon spectrum, multiple scattering, delta-ray production, relativistic rise and density correction [15], and the experimental trigger conditions.

Within the (mainly systematic) errors, theory and data agree very well. Over two decades in energy, deviations from exact linearity, which would manifest themselves via an energy dependence of $E_{\text{scint}}/E_{\text{kin}}$, are below 10%, and compatible with zero.

Fig. 6 demonstrates that the $1/\sqrt{E}$ dependence of the energy resolution holds approximately for about three decades in energy – note that the absolute width of the pulse-height distribution changes by a factor 25 for the energy range covered by the data points. At high energies, slight deviations due to leakage are observed and are well accounted for the by the EGS Monte Carlo simulation.

4. Performance of the shower detector

4.1. Correction of raw data

In a storage ring detector, electrons and photons will not hit the detector in the center of an absorber stack, and parallel to its axis, but will be distributed uniformly, with angles of incidence up to 45° (corresponding to the range in polar angle of the ARGUS barrel shower counter). Transitions between two absorber stacks, as well as losses in the unsampled material in the support structure and enhancement by the wavelength shifter will broaden the overall performance, compared to the data shown in section 3. In this section, we will discuss the resolution of the calorimeter averaged over impact point and -angles.

For the data discussed in the following, all counters were calibrated using an electron beam hitting the center of a stack; all pulse height are measured in equivalent energy (in MeV). $E_{\text{vis}} = \Sigma E_i$ denotes the sum over the energies E_i deposited in each stack. $\tilde{x} = (\Sigma E_i x_i)/E_{\text{vis}}$ is the x-coordinate of the center of gravity of a shower, calculated using the center x_i of the ith stack, and similarly for the y-coordinate. For the definition of the coordinate system, see fig. 7. Note that the $z = 0$ plane lies 5 cm behind the front end of the calorimeter, exactly at the position of the shower center (fig. 2). This definition has the advantage that at fixed impact coordinates x, y the center $\tilde{x}$, $\tilde{y}$ of a shower is independent of the angle of incidence of the beam [for the energy range covered here, the variation of the z-coordinate of the shower center with $\ln(E)$ can be neglected].

Since the amount of scintillator light collected depends on the position of a shower within the calorimeter, E_{vis} is a function of the impact point of a particle, as demonstrated in fig. 8a. E_{vis} has a maximum for particles hitting the absorber close to a wavelength shifter. The rms width of the distribution in pulse heights is nearly constant (fig. 8b). Contrary to results at higher energies [2,3], the energy resolution does not worsen even in the most critical regions A,B (fig. 7). The explanation is simply that at energies below 40 MeV, sampling fluctuations are so large that they dominate all other effects. Even the position dependence of the pulse

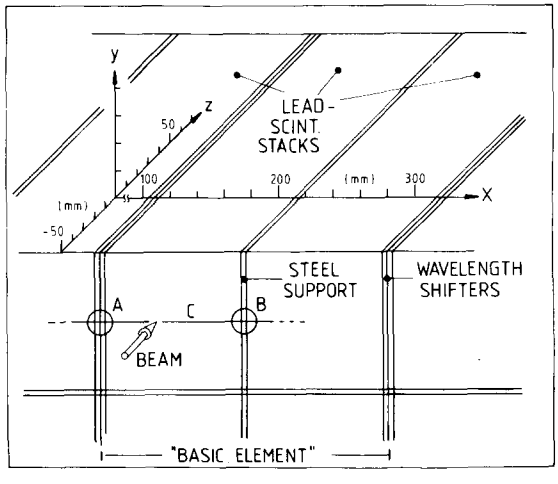

Fig. 7. Test setup: shows the definition of the coordinate system and of the so-called "basic element".

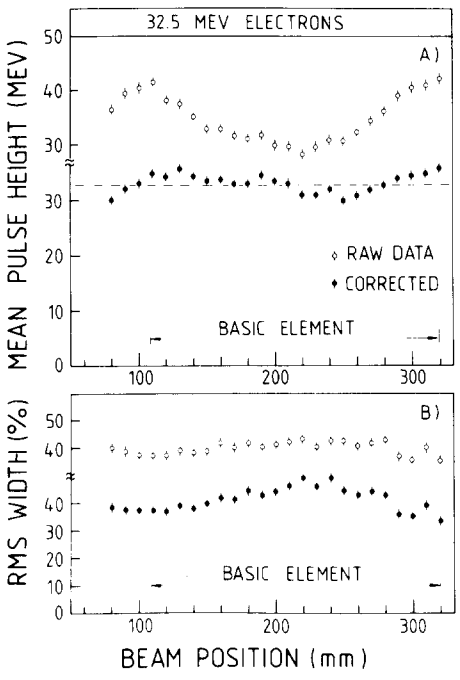

Fig. 8. Spatial scan: (A) Mean observed pulse height as a function of impact position, for a scan along line C in fig. 7. The electron beam is parallel to counter axis. Open points: raw data, closed points: corrected using the reconstructed impact point. (B) Rms energy resolution vs. impact position.

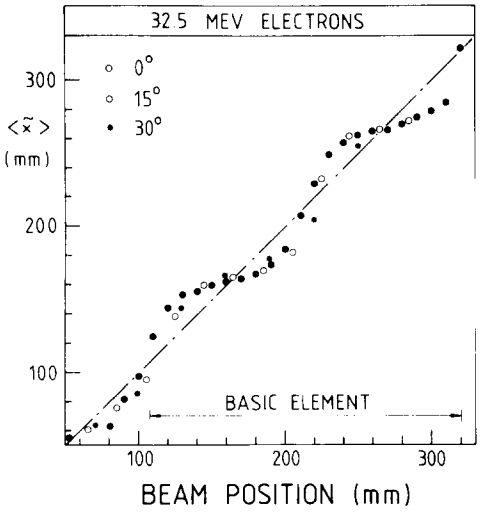

Fig. 9. Mean center of gravity of energy deposition as a function of impact position, for a scan along line C in fig. 7: Stars, open and closed circles refer to various angles of incidence with respect to the counter axis; the beam axis is always parallel to the $x-z$ plane.

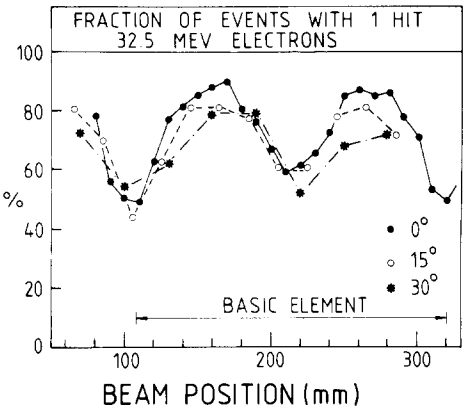

Fig. 10. Fraction of events with only one "hit" in the calorimeter array as a function of impact position, for various angles of incidence: The number of hits is defined as the number of absorber stacks, each of which contains at least 10% of the total energy deposited in the calorimeter array.

height (< 15% rms) has negligible influence on the overall energy resolution (> 30% rms).

Nevertheless, one might prefer to correct this position dependence in order to avoid possible systematic biases. Such a correction is in fact possible, since the impact point of a particle can be reconstructed from the measured shower center $\tilde{x}$, $\tilde{y}$. Fig. 9 shows $\tilde{x}$ as a function of the beam position x. $\langle \tilde{x} \rangle$ is a nonlinear function of x, since for particles not too close to a stack boundary, in most cases one stack contains the entire energy (fig. 10), and all $\tilde{x}$ are pulled towards the x_i of this stack.

Nevertheless, corrected values for energy and position can be derived using

$$x = \tilde{x} + F(\tilde{x}), \quad y = \tilde{y} + F(\tilde{y}), \quad E = E_{\text{vis}} G(\tilde{x}, \tilde{y}), \quad (3)$$

where F and G are periodic functions, which can be derived from the data shown in figs. 8a and 9, and which can be represented by a Fourier series. Within the precision required here, F and G are independent of the particles energy and angle of incidence. (The latter property is due to the proper choice of the origin of the coordinate system, see fig. 7.)

Fig. 8a shows the corrected mean pulse height. Since the correction translates radial fluctuations in the shower development into energy fluctuations, the rms energy resolution slightly worsens (fig. 8b).

4.2. Average performance

We are now prepared to summarize the performance of the shower counter system, averaged over impact coordinates and -angles.

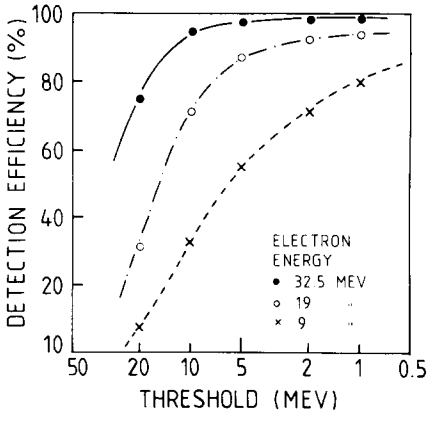

Fig. 11. Detection efficiencies for 9, 19, and 32.5 MeV electrons as a function of a (software) threshold: An electron is "detected", when the energy deposition in at least one absorber stack exceeds the threshold. Since especially the 9 MeV data include a few percent of fake triggers, the efficiencies shown should be considered as lower limits. Data averaged over impact points and -angles.

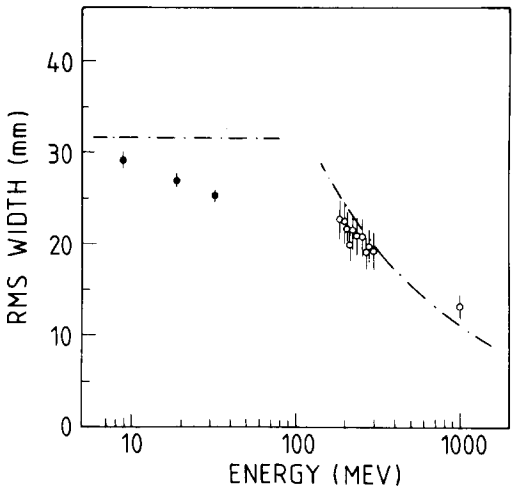

Fig. 12. Accuracy of reconstruction of the x-coordinate of the impact point, averaged over impact positions and -angles.

4.2.1. Detection efficiency

As mentioned in the introduction, one of the design aims was to achieve a very low detection threshold for electromagnetic showers. Fig. 11 shows the detection efficiencies for three different electron energies, as a function of the energy threshold. A particle is detected, when the energy deposition in at least one stack exceeds this threshold. In the test setup, which was positioned close to the Betatron, a threshold as low as 0.5 MeV could be used, without any problems due to pedestal drift, electronics and PM noise, and induced rf signals. The insensitivity to induced signals is due to a special design of the PM base, employing decoupled signal- and hv grounds [16]. In the environment of a storage ring, thresholds of 1–2 MeV should be managable, resulting in detection efficiencies > 97% for 30 MeV electrons resp. photons, and a low-energy cut-off below 10 MeV (for 50%. efficiency).

4.2.2. Energy resolution

Fig. 6 shows the average energy resolution for three electron energies (open points). Typical values are around $8\% \cdot \mathrm{GeV}^{1/2}$. The small insert shows a typical distribution of pulse heights averaged over impact positions and -angles. The peak at 0 is caused to a large extent by a few percent of false triggers in the data sample, nevertheless it has been included in the calculation of the rms width.

4.2.3. Spatial resolution

In fig. 12 the rms width of the distribution of the difference between reconstructed and true impact coordinate is shown, together with data points at higher energies [2,3]. Naively one expects a $\sqrt{E}$ dependence of the rms resolution. Fig. 12 proves that this simple-minded guess fails at low energies. A qualitative description of the data is however still possible using a $1/\sqrt{E}$ dependence at large energies, and assuming that in any case it is possible to find the stack which was hit by the incident particle, thereby limiting the resolution to $D/\sqrt{12}$ at low energies, where D is the width of one stack.

All these results refer to incident electrons. As far as calorimetry is concerned, almost all results should hold for incident photons as well.

In practical applications, the performance of the

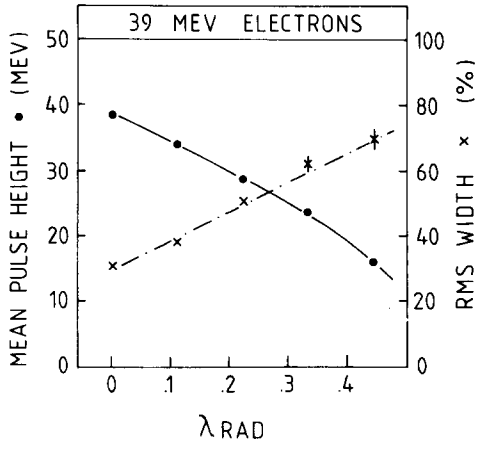

Fig. 13. Mean pulse height (●) and rms energy resolution (×) as a function of the thickness of absorber material (aluminum) in front of the counters, for 39 MeV electrons.

calorimeter may be worsened due to additional material in front of the calorimeter. In order to indicate the order of magnitude of possible effects, we show in fig. 13 the mean pulse height and the relative rms resolution obtained with various amounts of absorbing material (aluminum) placed in front of the detector. From Monte Carlo studies we expect that the decrease of mean pulse height and worsening of energy resolution will not be so strong for incident photons. In the ARGUS detector, the material in front of the counters amounts to 17% of a radiation length.

5. Conclusions

The various measurements discussed in this paper have proven that the rectangular modules of the ARGUS barrel shower counter behave almost like an ideal (sampling) calorimeter, as far as linearity and energy resolution are concerned. The device offers a dynamic range of 10^3 for the measurement of electron- and photon energies. Detection thresholds below 10 MeV seem feasible. Deviations from ideal behaviour at highest energies can be understood in terms of leakage.

In contrast to observations at GeV-energies, in the 10–40 MeV energy range the support structure and the modularity of the calorimeter do not induce sizeable inhomogeneities – this convenient but somewhat unexpected behaviour is explained by the fact that at these energies the resolution is entirely dominated by sampling fluctuations.

We acknowledge the skillful work of our technicians H. Höper, G. Metze and of our mechanical workshop in building the shower counters. We are indebted to Dr. M. Scherer, H.J. Büttner and T. Villet for their help to bring the Betatron into operation.

We thank our collegues and the technicians from ITEP, Moscow, who prepared the PM-bases and the related mechanics.

Special thanks go to the Freundesgesellschaft der Universität Dortmund for funding the Betatron.

One of us (W.H.) wants to thank the Deutsche Forschungsgemeinschaft for a Heisenberg Fellowship.

This work was supported by the Bundesministerium für Forschung und Technologie, FRG.

References

[1] W.A. Shurcliff, J. Opt. Soc. Am. 41 (1951) 209; R.C. Garwin, Rev. Sci. Instr. 31 (1960) 1010; G. Keil, Nucl. Instr. and Meth. 89 (1970) 111; A. Barish et al., Calt. 68–623 (1977); W. Selove et al., Nucl. Instr. and Meth. 161 (1979) 233; W.B. Atwood et al., SLAC-TN-76-7 (1976).
[2] W. Hofmann et al., Nucl. Instr. and Meth. 163 (1979) 77.
[3] W. Hofmann et al., Nucl. Instr. and Meth. 195 (1982) 475.
[4] ALTUSTIPE UV 15105, 84% PMMA, 15% Naphtalene, 1% Butyl-PBD, Altulor, Paris la Defense, France; L. Allemand et al., Nucl. Instr. and Meth. 164 (1979) 93.
[5] Plexiglas GS 218, 120 mg BBQ/l, Röhm GmbH, Darmstadt, FRG.
[6] Multiplier XP 2008 UB, Valvo, Hamburg, FRG.
[7] Nalophan, Kalle AG, Wiesbaden, FRG.
[8] A. Markees et al., to be published.
[9] W. Hofmann et al., to be published.
[10] R.L. Ford and W.R. Nelson, EGS version-3, SLAC-210, UC-32 (1978).
[11] U. Amaldi, Phys. Scripta 23 (1981) 409.
[12] S.L. Stone et al., Nucl. Instr. and Meth. 151 (1978) 387.
[13] ADC 2249 A, LeCroy, New York, USA.
[14] B. Rossi, High energy particles (Prentice Hall, New York, 1952).
[15] H. Bischel, URCL-17538, and Phys. Let. 50B (1974) 1.
[16] W. Heyde et al., Heidelberg-Report No. 4 (1974) unpublished.